ELSEVIER

Physics of the Earth and Planetary Interiors 114 (1999) 181–196

PHYSICS OF THE EARTH AND PLANETARY INTERIORS

The adjustment to Taylor's constraint in the presence of an ambient field

M.R. Walker [a,*], R. Hollerbach [b]

[a] *Department of Earth Sciences, Leeds University, Leeds LS2 9JT, UK*
[b] *Department of Mathematics, University of Glasgow, Glasgow G12 8QW, UK*

Received 11 March 1998; received in revised form 27 October 1998; accepted 5 March 1999

Abstract

The need to satisfy Taylor's constraint is probably the single most important constraint on the dynamics of planetary magnetic fields. We point out that the adjustment to Taylor's constraint is considerably more difficult in the Galilean moons of Jupiter than in the Earth, e.g., simply due to the presence of the ambient Jovian field. In particular, if the ambient field is of sufficient strength, weak field solutions are disallowed. The 'default option' of falling back to an Ekman state, if Taylor's constraint cannot be satisfied in any other way, is therefore no longer available. The magnetic field *must* therefore be in a Taylor state, a model-Z state, or something else entirely, but it *cannot* be in an Ekman state. In this work, we present a simple model of magnetoconvection specifically designed to explore this adjustment to Taylor's constraint in the limit of vanishing viscosity, in the presence of an ambient field. We find that for a weak imposed thermal wind, the system approaches a Taylor state as the strength of the ambient field is increased. Strong thermal wind solutions behave in a very different manner. Initially, as the ambient field strength is increased, the system exhibits many features, indicating that a Taylor state is being approached. However, it never reaches a Taylor state, evolving instead to a model-Z state as the ambient field strength is increased yet further.

Keywords: Taylor's constraint; Dynamo; Jovian moons

1. Introduction

The Galileo mission to Jupiter has revealed some interesting results, none more than the discovery that some of the Jovian moons possess magnetic fields of their own. Prior to this mission, the only two terrestrial objects known to have magnetic fields were the Earth and Mercury, although both Mars and the moon are thought to have had active dynamos in the past (Russell, 1993). The new data have revealed that of the four Galilean moons, Io, Europa, Ganymede and Callisto, only Callisto does not have its own magnetic field (Kivelson et al., 1996a,b; Khurana et al., 1997), although there is very little evidence that Europa houses its own intrinsic field (Khurana et al., 1998). It is therefore of some interest to consider not just the origin of these fields, but

* Corresponding author. Tel.: +44-1132336620; fax: +44-1132335259; e-mail: m.walker@earth.leeds.ac.uk

0031-9201/99/$ - see front matter
PII: S0031-9201(99)00059-X

also their subsequent equilibration in the background Jovian field.

Direct numerical simulations of dynamo action in the presence of an ambient field have been performed by Sarson et al. (1997), who considered Io and Ganymede in particular. They found that for the case of Ganymede, the ambient field is of secondary importance, in that Ganymede's own field does not decay if the ambient field is removed (although its structure is altered somewhat). For the case of Io, however, they found that its field decayed if the ambient field was removed, i.e., Io does not seem to be acting as a genuine dynamo, but is instead merely amplifying the pre-existing field. Their model, though simple in some ways (only dipole-type solutions of 2.5 dimensions were considered; Jones et al., 1995), clearly shows that the ambient field can play a crucial role in maintaining the intrinsic field of the Galilean moons.

However, one very serious limitation, not just in the model of Sarson et al. (1997) but in all numerical simulations of self-consistent planetary dynamos carried out to date (Glatzmaier and Roberts, 1997; Kuang and Bloxham, 1997), is that numerical difficulties prevent physically realistic values of the Ekman number being reached (see Walker et al., 1998). [The Ekman number E, measuring the ratio of viscous to Coriolis forces, is defined as $E = \nu/2\Omega R^2$, where ν is viscosity, Ω rotation rate and R core radius.] In the cores of the Galilean moons, the precise values of the viscosity ν are obviously not available. However, assuming a viscosity comparable with that assumed for the Earth's core ($\nu = 3 \times 10^{-6}$ m^2 s^{-1}), and using the rotation rate and estimated core radius of either Io ($\Omega = 4.11 \times 10^{-5}$ s^{-1}, $R = 950$ km), or Ganymede ($\Omega = 1.01 \times 10^{-5}$ s^{-1}, $R = 660$ km), E can be no larger than 10^{-13}. [Note: if turbulent viscosities are assumed, this can be increased to $O(10^{-9})$.] In the numerical simulations mentioned above, the Ekman number cannot be reduced much beyond 10^{-4}, at least not without resorting to hyperviscosities, the use of which presents serious problems of its own (Zhang and Jones, 1997). Thus, it is not clear how relevant the numerical simulations at $E \geq O(10^{-4})$ are to the physically realistic systems of $E \leq O(10^{-13})$, or $E \leq O(10^{-9})$ if turbulent viscosities are assumed. This is particularly true in light of the fact that there is a well-known constraint, Taylor's constraint, which must be satisfied in the limit $E \to 0$.

This gives the physical motivation for the mathematical problem investigated in this paper: we consider the simplified problem of the evolution of an axisymmetric magnetic field in the presence of an imposed ambient field. Although the model described below is only broadly applicable to Jupiter's moons, it remains of theoretical interest as the fully three-dimensional problem is computationally intractable using present-day technology. From a theoretical viewpoint, this problem is very appealing since the presence of the ambient field allows the anti-dynamo theorem of Cowling (1934) to be circumvented; i.e., a purely axisymmetric field can be maintained by (in the model described below) axisymmetric motions, simply because the imposed ambient field provides a continuous source of poloidal field which is required to complete the dynamo cycle. Also, the ambient field implies that the somewhat ambiguous α-effect, which has to be applied in an ad-hoc manner in mean-field dynamo models, can be omitted from this model. (See Hollerbach, 1996 for a review of mean-field dynamo theory.) The absence of any source of poloidal field other than the imposed field does mean, however, that in this model, a poloidal field of significantly stronger field strength than that of the imposed field can never be obtained, whereas in some of the Jovian moons, the internal fields are stronger than the external field.

In the dimensionless momentum equation in a rapidly rotating planetary core, both the Rossby number (Ro $= \eta/2\Omega R^2$, measuring the ratio of inertial to Coriolis forces, where $\eta = 1$ m^2 s^{-1} is magnetic diffusivity), and Ekman number E are extremely small, so small that it is tempting to neglect inertia and viscosity entirely. However, in this so-called magnetostrophic approximation (Ro $\equiv 0$, $E \equiv 0$), the momentum equation, in general, has no solution at all. It will only have a solution if the constraint of Taylor (1963) is satisfied, stating that the Lorentz torque integrated over geostrophic contours vanishes (the geostrophic contours being concentric cylindrical shells parallel to the axis of rotation). Furthermore, even if this constraint is satisfied, so that the momentum equation has a solution, that solution is only determined within an arbitrary

geostrophic flow $U_g(s)\hat{\phi}$, consisting of geostrophic cylinders rotating as if they were solid shells.

One way of relaxing this constraint is to reintroduce viscosity, but only in the Ekman boundary layers. This also has the advantage of yielding an explicit expression for the geostrophic flow:

$$U_g(s) = E^{-1/2} \frac{(1-s^2)^{1/4}}{2\sqrt{2}\,\pi s} \int [(\nabla \times \mathbf{B}) \times \mathbf{B}] \cdot \hat{\phi} \mathrm{d}S, \quad (1.1)$$

where the integration is performed over the geostrophic cylinders, and s is the perpendicular distance from the rotation axis. See, e.g., Fearn (1994) or Hollerbach (1996) for the details of this derivation. Note that Eq. (1.1) is only valid for a full sphere; for simplicity, we do not include a solid inner core, thus avoiding possible complications associated with the inner core tangent cylinder (Hollerbach and Proctor, 1993).

If $I(s)$ were $O(1)$, where $I(s)$ is defined as:

$$I(s) \equiv \int [(\nabla \times \mathbf{B}) \times \mathbf{B}] \cdot \hat{\phi} \mathrm{d}S, \quad (1.2)$$

the geostrophic flow would diverge as $O(E^{-1/2})$; which turns out to be energetically unsustainable (see, e.g., Barenghi and Jones, 1991; Hollerbach and Ierley, 1991; Hollerbach, 1996). Thus, we obtain the viscous version of Taylor's constraint, stating that the integrated Lorentz torque $I(s)$ does not have to vanish identically, but it does have to tend to zero as E tends to zero. The only remaining question then is how this adjustment comes about.

The simplest way of satisfying $I = O(E^{1/2})$, and thereby yielding a non-divergent geostrophic flow, would be to have the field scale as $O(E^{1/4})$—the so-called Ekman state. While this option has the advantage that no adjustment is required in the structure of the field, it has the disadvantage that the field is very weak. For example, in Io, if the field were in an Ekman state, with $E = 10^{-13}$, the dimensionless field strength can at most be $O(10^{-4})$; scaled to its dimensional value, this gives a field of strength $O(10^{-7}$ T). [The field scale is given by $(2\Omega\mu_0\rho\eta)^{1/2}$. Ω and η are given above, μ_0 is the permeability of free space and ρ the density (5150 kg m^{-3} for both Io and Ganymede).]

Alternatively, it is possible have an $O(1)$ field, and still satisfy $I = O(E^{1/2})$, provided that sufficient internal cancellation occurs in the integral (Eq. (1.2)). This is known as a Taylor state. While this option has the advantage of yielding a strong field, it has the disadvantage that a very special adjustment in the structure of the field is required to give such an exact cancellation. In a physical system, a Taylor state may naturally, and possibly quite easily, occur but it has been shown that Taylor states are notoriously difficult to achieve in any planetary dynamo model. One reason for this difficulty is simply that the natural coordinate system for the evaluation of Eq. (1.1) is cylindrical, whereas the natural coordinates for the dynamo problem are spherical. This, together with the fact that the effect of Eq. (1.1) on the energy balance is a negative semi-definite function (i.e., it is a sink of energy), and that it must remain so throughout any simulation, has previously caused much computational difficulty due to numerical instabilities. However, following Walker and Barenghi (1998), we are able to evaluate Eq. (1.1) both efficiently and to a high degree of accuracy and thus examine the possible transition to a Taylor state—a regime which is of interest as it implies a strong field solution.

One final state that the system could evolve to is that I could tend to zero more slowly than $O(E^{1/2})$, which will course yield a divergent geostrophic flow. Energetically, this is still allowed, provided it does not diverge as strongly as $O(E^{-1/2})$, and provided also that the magnetic coupling between the geostrophic cylinders is sufficiently weak. The way to ensure the magnetic coupling is sufficiently weak is to have a field where B_ϕ and B_z are $O(1)$, but B_s is small (B_s, B_ϕ, B_z are the field components in cylindrical geometry). This scenario, first suggested by Braginsky (1975), is referred to as model-Z, because the B_z, B_s parts of the field are thus aligned with the z-axis. (See also Braginsky, 1994 for a review of model-Z.) Although originally proposed as a model for the geodynamo, it is now widely believed that the Earth's field is probably not in a model-Z state: the self-consistent simulations (Glatzmaier and Roberts, 1997; Kuang and Bloxham, 1997) certainly show no particular tendency for the

field to align with the z-axis. However, in this work, we will show that model-Z may be relevant to the evolution of a magnetic field in the presence of an ambient field.

To summarise, there are three different states—the Ekman, Taylor, and model-Z states—that the system could adopt. Two of these, the Taylor and model-Z states, are associated with $O(1)$ field strengths, and are therefore particularly desirable. However, because both of them require particular adjustments in the structure of the field, they may not always be achievable. The traditional view of planetary dynamos has then been that if either of these states is achievable, the system will adopt that state (with the Taylor state probably taking precedence over the model-Z state if both are achievable), but if (perhaps only temporarily) neither is achievable, the system will simply fall back to the Ekman state. For example, both Hollerbach et al. (1992) and Hollerbach and Jones (1995) obtained solutions in which the field strength temporarily dropped quite substantially, possibly indicating such a collapse back to the Ekman state. However, once the imposed ambient field strength is greater than $O(E^{1/4})$, the Ekman state is not accessible, even just temporarily. The solution must therefore be in a Taylor state, or a model-Z state, or something else entirely (such as a semi-Taylor state perhaps in which the field scales as $O(E^{1/8})$; Hollerbach, 1997), but it does not have the option of falling back to the Ekman state if it cannot satisfy Taylor's constraint in any other way. The purpose of this work is thus to explore the adjustment to Taylor's constraint in the presence of an ambient field when the 'default option' of the Ekman state is not available.

A brief outline of the paper is the following. A mathematical description of the model is given in Section 2, while Section 3 is reserved for results. Finally, in Section 4, we summarise our findings and discuss some possible implications for the Galilean moons of Jupiter.

2. The model

In order to facilitate an exploration of the very small E limit, we consider a model far simpler even than that of Sarson et al. (1997), let alone the fully three-dimensional simulations of Glatzmaier and Roberts (1997) or Kuang and Bloxham (1997). In particular, we consider a purely axisymmetric model, and do not solve for the details of the convection at all, but simply prescribe the mean buoyancy force. The equations we solve are given by:

$$\hat{z}\times\mathbf{U} = -\nabla P + E\nabla^2\mathbf{U} + (\nabla\times\mathbf{B})\times\mathbf{B} + \Theta\hat{r}, \tag{2.1}$$

$$\frac{\partial\mathbf{B}}{\partial t} = \nabla\times(\mathbf{U}\times\mathbf{B}) + \nabla^2\mathbf{B}, \tag{2.2}$$

$$\nabla\cdot\mathbf{U} = 0, \quad \nabla\cdot\mathbf{B} = 0, \tag{2.3}$$

where $\mathbf{B}$ is the total magnetic field, including the externally imposed part, $\mathbf{U}$ is the fluid flow, and Θ is the kinematically prescribed buoyancy force. We also expand $\mathbf{U}$ and $\mathbf{B}$ as:

$$\mathbf{U} = U\hat{\phi} + \nabla\times\left(\psi\hat{\phi}\right), \quad \mathbf{B} = B\hat{\phi} + \nabla\times\left(A\hat{\phi}\right), \tag{2.4}$$

thereby automatically satisfying Eq. (2.3).

With these expansions in place, the momentum (Eq. (2.1)) becomes:

$$\frac{\partial\psi}{\partial z} + ED^2U = -N(B,A), \tag{2.5a}$$

$$\frac{\partial U}{\partial z} - ED^4\psi = M(B,B) + M(D^2A,A) + \frac{\partial\Theta}{\partial\theta}, \tag{2.5b}$$

where:

$$D^2 \equiv \nabla^2 - 1/(r\sin\theta)^2, \tag{2.6a}$$

$$M(f,g) \equiv \nabla\times\left[f\hat{\phi}\times\left(\nabla\times g\hat{\phi}\right)\right]\cdot\hat{\phi}, \tag{2.6b}$$

$$N(f,g) \equiv \left[\left(\nabla\times f\hat{\phi}\right)\times\left(\nabla\times g\hat{\phi}\right)\right]\cdot\hat{\phi}. \tag{2.6c}$$

At any finite value of E, these equations can be solved directly, which is essentially what the more complicated models referred to above do. However, computationally, the Ekman number cannot be reduced much beyond 10^{-4}, because the various boundary and internal layers which must be resolved become too thin. In order to explore the adjustment to Taylor's constraint, E must be reduced well beyond 10^{-4}, and so a different approach is required.

Rather than solve Eqs. (2.5a) and (2.5b) directly, it is solved asymptotically, including the viscous terms only in the Ekman boundary layers and, using the known structure of these layers, this results in the following equations for the axisymmetric flow:

$$\psi = -\int_0^z N(B,A)\,\mathrm{d}z', \tag{2.7}$$

$$U = U_\mathrm{m} + U_\mathrm{t} + U_\mathrm{g}(s), \tag{2.8}$$

where:

$$U_\mathrm{m} = -\int_z^{z_\mathrm{T}} \big(M(B,B) + M(D^2A,A)\big)\,\mathrm{d}z' \tag{2.9}$$

is the magnetic wind,

$$U_\mathrm{t} = -\int_z^{z_\mathrm{T}} \frac{\partial \Theta}{\partial \theta}\,\mathrm{d}z' \tag{2.10}$$

is the thermal wind, and $U_\mathrm{g}(s)$ is the geostrophic flow given by Eq. (1.1), which, for purely axisymmetric fields, can also be written as:

$$U_\mathrm{g}(s) = -E^{-1/2}\frac{(1-s^2)^{1/4}}{\sqrt{2}\,s^2}\frac{\mathrm{d}}{\mathrm{d}s} \times\left[s^2\int_{-z_\mathrm{T}}^{+z_\mathrm{T}} B\frac{\partial A}{\partial z}\,\mathrm{d}z\right], \tag{2.11}$$

where (s,ϕ,z) are cylindrical coordinates and $z_\mathrm{T} \equiv (1-s^2)^{1/2}$.

Once again, readers are referred to Fearn (1994) or Hollerbach (1996) for more details. The great advantage of this method is that, because the Ekman layers need no longer be explicitly resolved, there is no need to increase the resolution as E decreases, allowing far smaller values of E to be reached.

Using Eq. (2.4), the induction of Eq. (2.2) becomes:

$$\frac{\partial A}{\partial t} = D^2A + N(\psi,A), \tag{2.12a}$$

$$\frac{\partial B}{\partial t} = D^2B + M(U,A) - M(B,\psi). \tag{2.12b}$$

The poloidal and toroidal field components A and B are further expanded in Legendre functions as:

$$A = \sum_{n=1}^{N} a_n(r)\,P_{2n-1}^1(\cos\theta),$$

$$B = \sum_{n=1}^{N} b_n(r)\,P_{2n}^1(\cos\theta), \tag{2.13}$$

and, incidentally, here we have restricted attention to only dipole-type solutions having A (and U) symmetric and B (and ψ) antisymmetric about the equator.

The expansion (Eq. (2.13)) is particularly convenient for matching A to an external potential, which is also how the externally imposed field is introduced. If there is no external field, the boundary conditions on the $a_n(r)$ would simply be:

$$\frac{\mathrm{d}a_n(r)}{\mathrm{d}r} + \frac{2n}{r}a_n(r) = 0, \text{ at } r = 1. \tag{2.14}$$

To include the externally imposed field, simply change Eq. (2.14) for a_1 and a_2 to:

$$\frac{\mathrm{d}a_1(r)}{\mathrm{d}r} + \frac{2}{r}a_1(r) = -\frac{3}{2}B_\mathrm{p}, \text{ at } r = 1, \tag{2.15a}$$

$$\frac{\mathrm{d}a_2(r)}{\mathrm{d}r} + \frac{4}{r}a_2(r) = \frac{14}{45}CB_\mathrm{p}, \text{ at } r = 1, \tag{2.15b}$$

which then matches the imposed field:

$$A^* = B_\mathrm{p}\left(-\frac{1}{2}rP_1^1 + \frac{2}{45}Cr^3P_3^1\right). \tag{2.16}$$

See also Sarson et al. (1999), who similarly impose an ambient field via inhomogeneous boundary conditions on A. Except for the inhomogeneous boundary conditions (Eqs. (2.15a) and (2.15b)), the rest of the numerical procedure is exactly as described by Walker and Barenghi (1998): Eqs. (2.12a) and (2.12b) is time-stepped until the equilibrium solutions are reached (which turn out to be steady for all runs presented here), and at each time-step, ψ and U are evaluated directly according to Eqs. (2.7), (2.8), (2.9), (2.10) and (2.11).

The particular choice (Eq. (2.16)) of the externally imposed field requires some explanation at this point. If we had taken, following Sarson et al. (1997, 1999), simply:

$$A^* = B_\mathrm{p}\left(-\frac{1}{2}rP_1^1\right) = B_\mathrm{p}\left(\frac{1}{2}r\sin\theta\right) = B_\mathrm{p}\left(\frac{1}{2}s\right), \tag{2.17}$$

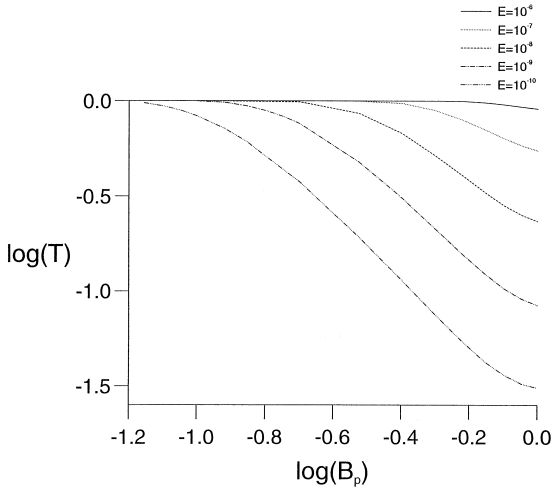

Fig. 1. The logarithm of the Taylorisation plotted as a function of B_p. $\omega_0 = 20$, $C = 1/15$, and ω is given by Eq. (2.18a).

according to Eq. (2.4), this would yield a purely axial field $\mathbf{B} = B_p \hat{z}$. Eq. (2.11) then implies a field in the form of Eq. (2.17), satisfying $\partial A/\partial z \equiv 0$, is degenerate and satisfies Taylor's constraint exactly. However, the result that a z-independent poloidal field automatically satisfies Taylor's constraint *only* applies if it is axisymmetric and insulating boundary conditions are employed. For a fully three-dimensional field, and including a conducting solid inner core and/or a weakly conducting mantle, even a z-independent poloidal field will not satisfy Taylor's constraint automatically (Fearn and Proctor, 1992). In the model presented here, this degeneracy occurs only because we work with such an idealised system. However, within the confines of this model, we clearly have to do something about this degeneracy. The simplest thing to do is to include a little curvature to the externally imposed field, so that it is still basically aligned with the z-axis, but not perfectly. Including this curvature in the imposed field is thus the reason for including the next higher harmonic P_3^1 in Eq. (2.16), with this (small) parameter C measuring the amount of curvature.

Finally, we note that according to Eq. (2.10), prescribing a buoyancy force Θ is equivalent to prescribing a thermal wind U_t. Following Roberts (1972), we will consider the two choices:

$$\omega = \omega_0 r, \tag{2.18a}$$

$$\omega = -\omega_0 \frac{3}{8}\sqrt{3}\,(1-r^2)^2, \tag{2.18b}$$

where $\omega = U_t/s$ is the angular velocity.

To summarise the model: given the imposed poloidal field (Eq. (2.16)), the thermal wind (Eqs. (2.18a) and (2.18b)) will act on it to induce a toroidal field via the term $M(U,A)$ in Eq. (2.12b)—the well-known ω-effect. For both choices of thermal wind (Eqs. (2.18a) and (2.18b)), the initial toroidal field B turns out to be of one sign throughout the entire upper hemisphere. Since the initial $\partial A/\partial z$ is also of one sign throughout the entire upper hemisphere, there will be no cancellation in the Taylor integral (Eq. (2.11)). As long as $B_p \le O(E^{1/4})$, this causes no problems, and A and B should remain essentially unchanged. However, as soon as $B_p \ge O(E^{1/4})$, the lack of cancellation will start to induce a very large geostrophic flow, which will act back on B, presumably distorting it in such a way that Taylor's constraint is then beginning to be satisfied. [At the same time, of course, the meridional circulation (Eq. (2.7)) is acting on both A and B, so A will also be distorted. However, because the dominant nonlinearity is the geostrophic flow, and because this acts only on B, we expect at least the initial adjustment to Taylor's constraint to come about by a distortion of B.] What we are thus interested in exploring is how the final equilibrated solutions behave as we gradually increase B_p beyond $O(E^{1/4})$, keeping all other parameters fixed.

The diagnostic quantity we compute to see how the solutions are behaving is the so-called Taylorisation parameter:

$$\mathcal{T} = \int_0^1 \left| \int_{z_B}^{z_T} B \frac{\partial A}{\partial z}\,\mathrm{d}z \right| \mathrm{d}s \Big/ \int_0^1 \int_{z_B}^{z_T} \left| B \frac{\partial A}{\partial z} \right| \mathrm{d}z\,\mathrm{d}s. \tag{2.19}$$

$\mathcal{T}$ is thus a measure of the internal cancellation in Eq. (2.11). From the point noted above, that for

Fig. 2. Contour plots of the dimensionless equilibrated field. Parameters as Fig. 1 with $B_p = 1$. Left-hand side illustrates $Ar\sin\theta$, right-hand side B. (a) $E = 10^{-6}$, $(Ar\sin\theta)_{max} = 0.5$, $B_{max} = 0.06$; (b) $E = 10^{-8}$, $(Ar\sin\theta)_{max} = 0.5$, $B_{max} = 0.035$, $B_{min} = -0.015$; (c) $E = 10^{-10}$, $(Ar\sin\theta)_{max} = 0.5$, $B_{max} = 0.035$, $B_{min} = -0.015$.

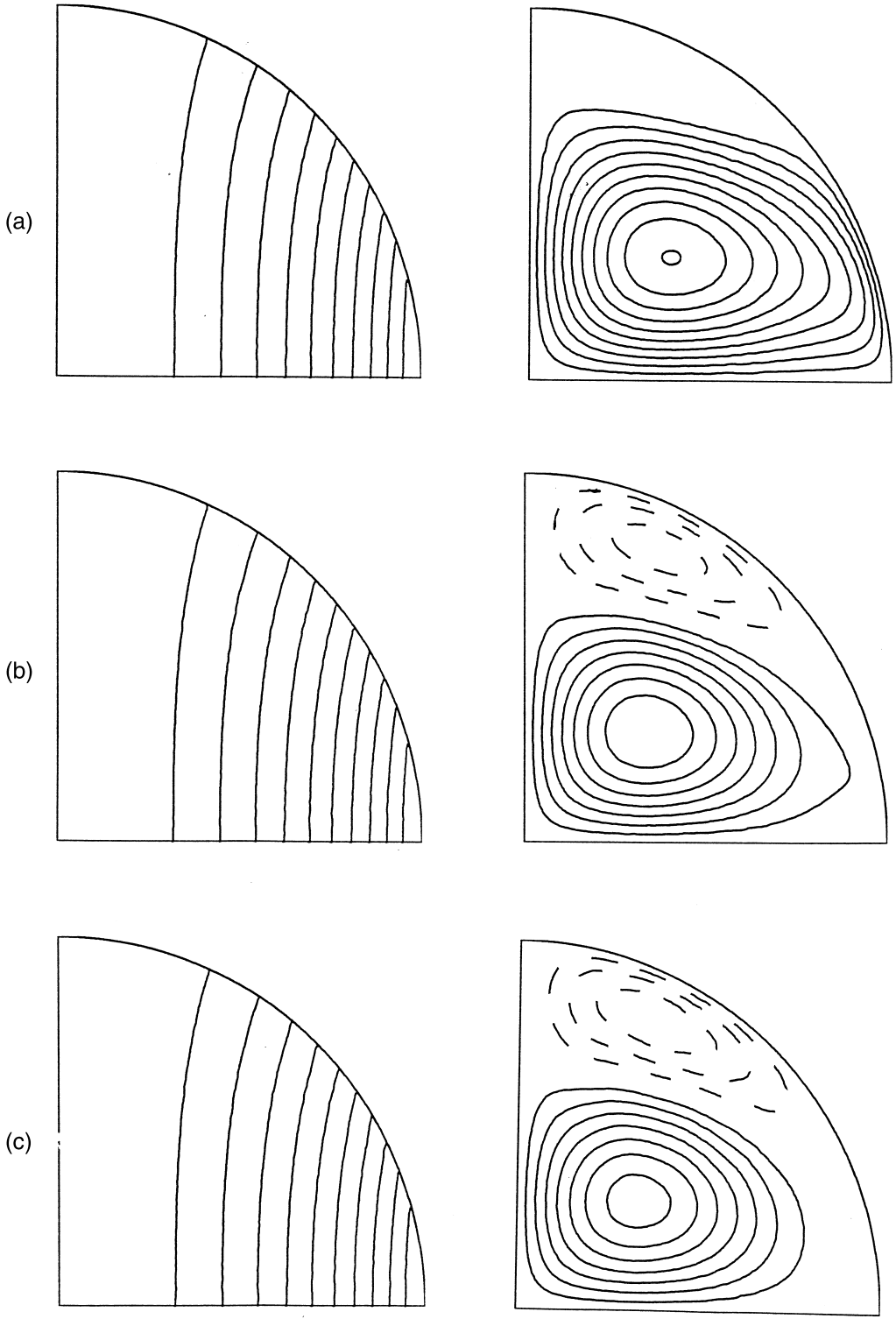
(a)
(b)
(c)

infinitesimal B_p, B and $\partial A/\partial z$ each has the same sign throughout the entire hemisphere, we conclude that initially $\mathscr{T}$ will be 1. But again, we know that as soon as B_p exceeds $O(E^{1/4})$, some sort of adjustment must occur. If the system evolves toward a Taylor state, $\mathscr{T}$ should eventually scale as $O(E^{1/2})$, whereas if it evolves toward a model-Z state, $\mathscr{T}$ should scale somewhere in between 1 and $O(E^{1/2})$. By repeating the process of gradually increasing B_p for a range of Ekman numbers, and observing how the Taylorisation behaves, we should be able to obtain some indication as to what state the system is tending to. (Of course, a direct observation of the solution will also prove invaluable. For example, the fact that, as E tends to zero the geostrophic flow is non-divergent in a Taylor state, but divergent in a model-Z state, will also help distinguish between the two.)

3. Results and discussion

3.1. Weak thermal wind solutions

We consider the cases $\omega_0 = 10$, 20, 30 with $C = 1/15$ and ω given by Eq. (2.18a). A similar qualitative picture emerges for all three cases, so to save space, we illustrate only one, namely $\omega_0 = 20$. In Fig. 1, we plot the logarithm of the Taylorisation, $\mathscr{T}$, against the logarithm of the imposed field strength, B_p, for Ekman numbers ranging from 10^{-6} to 10^{-10}. We find that $\log(\mathscr{T})$ does indeed become non-zero when $B_p = O(E^{1/4})$, with the precise value being independent of ω_0, incidentally.

Fig. 1 clearly shows that cancellation in the integrated Lorentz torque occurs to a greater extent, at given B_p, as the Ekman number is reduced. More importantly though, even in this model where the field lines are greatly restricted by the imposed field, the system is tending towards a Taylor state. In a Taylor state, $\log(\mathscr{T})$ should be reduced by 0.5 every time E is reduced by a factor of 10, which is clearly not the case yet for $E \geq 10^{-7}$, but tending to that for $E \leq 10^{-8}$. We note, however, that this system finds it harder to evolve to a Taylor state (i.e., we require a smaller E) than the mean-field dynamo models of Hollerbach and Ierley (1991) or Walker and Barenghi (1998), which typically required only $E \leq 10^{-6}$ to achieve an $O(E^{1/2})$ scaling in $\mathscr{T}$, whereas we require $E \leq 10^{-8}$. This is presumably because in this model, the field has to adjust almost exclusively by distorting B (as noted above), whereas in the mean-field dynamo models, it can adjust by distorting both A and B simultaneously.

To examine the approach to a Taylor state as the Ekman number is reduced, we illustrate the equilibrated solutions in Figs. 2 and 3. [Note: in all contour plots, solid (dashed) lines indicate positive (negative) regions. Unless equal to zero, the maximum and minimum values of the quantity plotted are given in the figure captions.] Comparing plots of the poloidal field (Fig. 2), we see that there is no observable difference in $Ar\sin\theta$ as we reduce the Ekman number from $E = 10^{-6}$ down to $E = 10^{-10}$; in all cases, the final equilibrated field is dominated by the imposed field. Since A is essentially fixed by the imposed field, this only leaves B as a free parameter if a Taylor state is to be reached. Examining plots of the toroidal field (still Fig. 2), we see that for $E = 10^{-8}$, 10^{-10}, the solution consists of two regions; a positive region at lower latitude (solid contours) and a negative region at higher latitude (dashed contours). This is in contrast to the solution at $E = 10^{-6}$ where the solution consists of a single large positive region. The crucial point we wish to stress here is that, since $\partial A/\partial z$ is of the same sign throughout the hemisphere for all E considered, the regions of positive and negative B appearing in the lower E solutions are essential for the internal cancellation in the integrated Lorentz torque, which is required if a Taylor state is to be reached. Finally, in Fig. 3, we illustrate the corresponding solutions for the magnetically driven part of the flow; the angular velocity $U/r\sin\theta$ (where $U = U_m + U_g$) and the meridional circulation $\psi r\sin\theta$. [We are not including the prescribed thermal wind U_t here to focus

Fig. 3. The dimensionless flow corresponding to Fig. 2. Left-hand side illustrates $U/r\sin\theta$ ($U = U_m + U_g$), right-hand side $\psi r\sin\theta$. (a) $E = 10^{-6}$, $(U/r\sin\theta)_{max} = 95$, $(\psi r\sin\theta)_{min} = -0.028$; (b) $E = 10^{-8}$, $(U/r\sin\theta)_{max} = 100$, $(\psi r\sin\theta)_{max} = 0.004$, $(\psi r\sin\theta)_{min} = -0.016$; (c) $E = 10^{-10}$, $(U/r\sin\theta)_{max} = 100$, $(\psi r\sin\theta)_{max} = 0.006$, $(\psi r\sin\theta)_{min} = -0.014$.

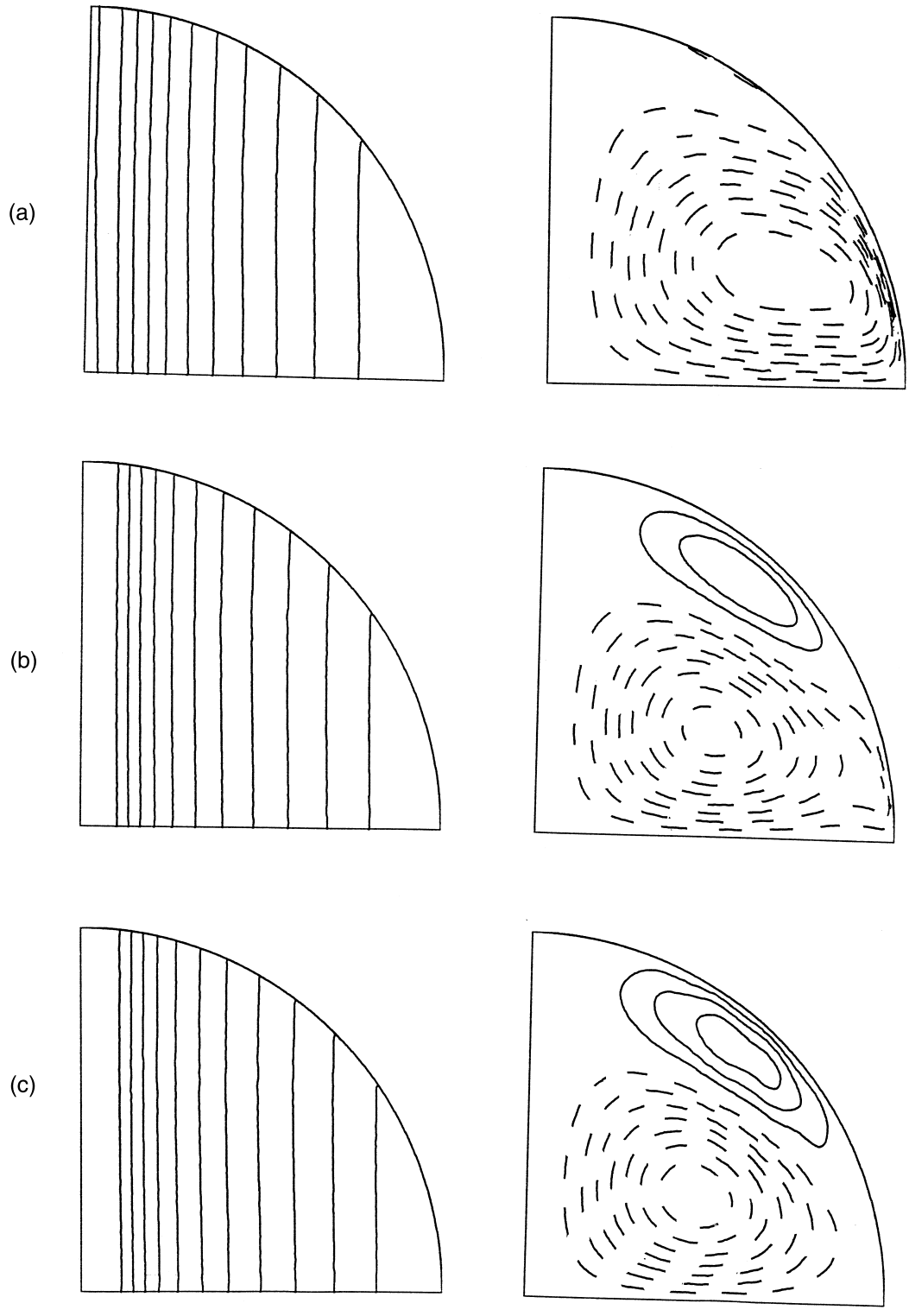
(a)
(b)
(c)

exclusively on the subsequent adjustment; however, Fig. 3 indicates that the magnitudes of $(U_m + U_g)/r\sin\theta$ and $U_t/r\sin\theta$ are comparable.] The morphology of the angular velocity is essentially unchanged for all E illustrated; more importantly though, its magnitude is unchanged as the Ekman number is reduced from $E = 10^{-8}$ down to $E = 10^{-10}$, indicating that the solution is indeed in a Taylor state.

3.2. Strong thermal wind solutions

The effect of increasing the strength of ω_0 is now investigated: with ω given by Eq. (2.18a), $C = 1/15$, we consider the cases $\omega_0 = 100$, 200, 400. In all three cases, results are qualitatively similar so again, to save space, we only give one example, namely $\omega_0 = 400$, although we make reference to the cases $\omega_0 = 100$, 200. In Fig. 4, we again plot the logarithm of the Taylorisation, $\mathcal{T}$, against the logarithm of the imposed field strength, B_p, for Ekman numbers ranging from 10^{-6} to 10^{-9}. We find that $\log(\mathcal{T})$ again becomes non-zero when $B_p = O(E^{1/4})$, with the precise value still being independent of ω_0.

For all E considered, as we increase B_p beyond $O(E^{1/4})$, cancellation begins to occur in the integrated Lorentz torque and $\log(\mathcal{T})$ decreases. However, unlike the weak thermal wind solutions, there is no evidence of a Taylor state being approached (i.e., the difference between successive curves is not

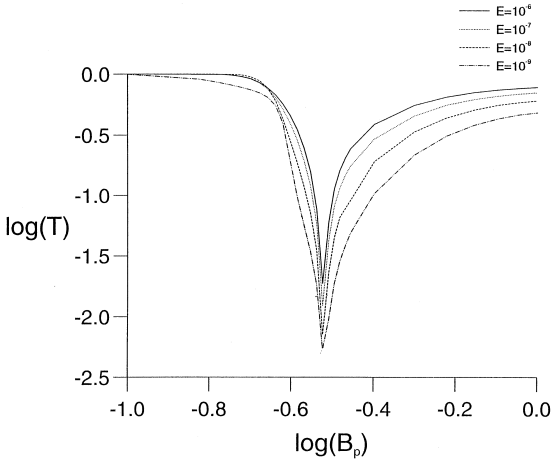

Fig. 4. As Fig. 1 with $\omega_0 = 400$.

tending to 0.5). For a given E, $\log(\mathcal{T})$ becomes more and more negative, reaching a minimum value at $B_p = B_p^{min}$, and then begins to increase, eventually tending towards a constant value as B_p is increased further yet. As already stated, this feature occurs for all three values of ω_0, although it is only for $\omega_0 > 200$ that B_p^{min} is exactly independent of E. To understand what happens as B_p is increased, it is informative to examine contour plots of the solution at large $B_p > B_p^{min}$, small $B_p < B_p^{min}$, and at $B_p = B_p^{min}$.

At large B_p, $\mathcal{T}$ tends to a constant value, for each E considered, but with the difference between successive curves considerably less than 0.5. Contour plots of the solution reveals some interesting features (Figs. 5 and 6). The field morphology of A differs significantly from A^*; more importantly though, as E is reduced, the field lines of A align themselves more and more with the z-axis (Fig. 5). This strongly suggests that the system has evolved to a model-Z state (Braginsky, 1994). Further evidence pointing to the model-Z nature of the solution can be found by examining the angular velocity (Fig. 6). $U/r\sin\theta$ is always dominated by its geostrophic part; more importantly though, it is of large magnitude, and increases with decreasing E. Examining the maximum amplitude of the azimuthal flow: $|U| = 245$, 385, 630, 1050 for $E = 10^{-6}$, 10^{-7}, 10^{-8}, 10^{-9}, respectively, implying that U_g is diverging as approximately $E^{-0.22}$, suggesting a possible asymptotic dependence of $E^{-1/4}$. However, solutions at even smaller E, which are beyond the scope of our numerical model, are required to confirm this scaling. Finally, plots of B and $\psi r\sin\theta$ indicate that both have large gradients close to the outer boundary, both characteristic of model-Z. With reference to $\psi r\sin\theta$, this indicates that there is a strong flow at the boundary layer—another clear indication that the system is indeed in a model-Z state.

For weak B_p, just beyond $O(E^{1/4})$, the solution departs from an Ekman state, as it must. The Taylorisation is then reduced as B_p is increased (for $B_p < B_p^{min}$). This indicates that internal cancellation in the integrated Lorentz torque occurs more and more. After B_p^{min}, $\mathcal{T}$ begins to increase with increasing B_p. What happens is that the evolution towards a Taylor state competes with the evolution towards a model-Z state. For small $B_p < B_p^{min}$ characteristics

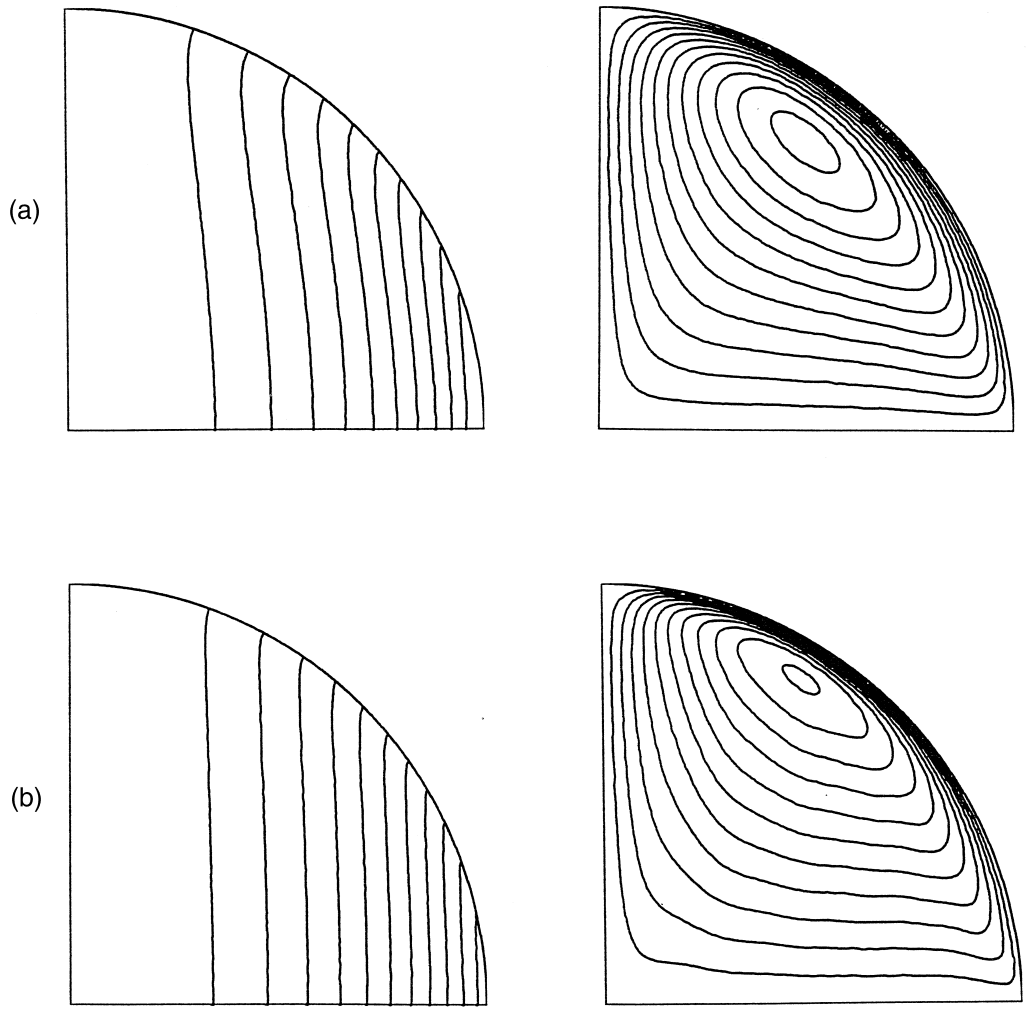

Fig. 5. As Fig. 2 with $\omega_0 = 400$. (a) $E = 10^{-6}$, $(Ar\sin\theta)_{max} = 0.45$, $B_{max} = 0.825$; (b) $E = 10^{-9}$, $(Ar\sin\theta)_{max} = 0.495$, $B_{max} = 0.66$.

indicating an evolution towards a Taylor state dominate (although a Taylor state is never reached), while for $B_p > B_p^{min}$, model-Z begins to dominate.

In Fig. 7, the magnetic field at $B_p = 0.24\ (< B_p^{min})$ and $B_p = 0.30\ (= B_p^{min})$ is plotted, while in Fig. 8, we plot the corresponding flow. For $B_p < B_p^{min}$ (Fig. 7a, Fig. 8a), where the preferred evolution is towards a Taylor state, B consists of a single large positive region and, crucially, in this case, A has been significantly modified from A^* in such a way that $\partial A/\partial z$ is no longer of the same sign throughout. This allows for cancellation in the integrated Lorentz torque and therefore $\mathscr{T} < 1$. This is in contrast to the weak thermal wind solution where A is always dominated by A^* and there it is the morphology of B which allows for Taylor states to be approached (see Fig. 2). The structure of the flow (Fig. 8a) is similar to the weak thermal wind solution (Fig. 3b), although its magnitude is now a factor of 10 or greater. Although the system is clearly not in a Taylor state at this stage, it does exhibit many features to suggest that it is evolving towards a Taylor state in the sense that, if the same features were to prevail as B_p is increased yet further (which obviously they do not), then a Taylor state would be reached. In conclusion, we merely state that the features appearing in the

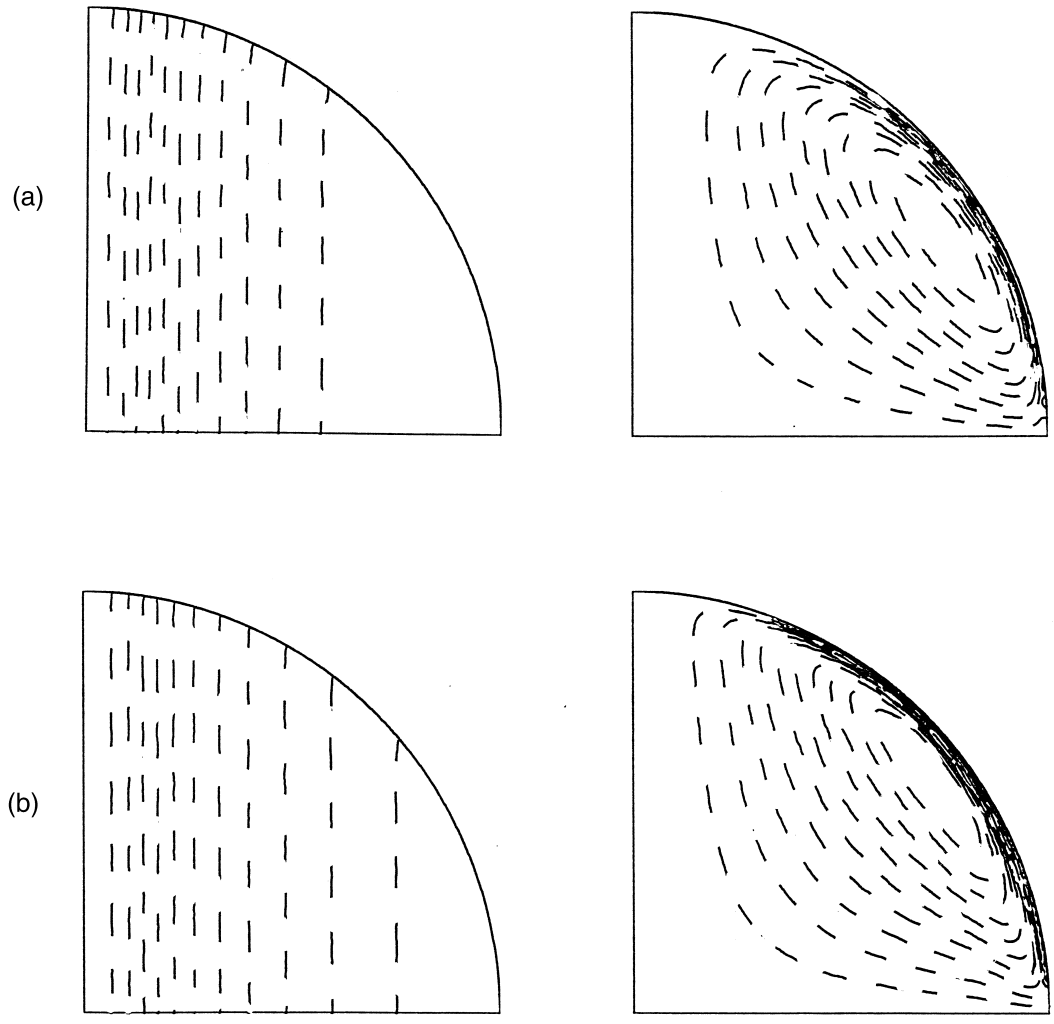

Fig. 6. As Fig. 3 with $\omega_0 = 400$. (a) $E = 10^{-6}$, $(U/r\sin\theta)_{\min} = -2200$, $(\psi r\sin\theta)_{\min} = -0.45$; (b) $E = 10^{-9}$, $(U/r\sin\theta)_{\min} = -9000$, $(\psi r\sin\theta)_{\min} = -0.35$.

solution here are indicative of the evolution towards a Taylor state. Contour plots of the solution at $B_p = 0.60$ (omitted here to save space) indicate that model-Z dominates; the solution resembles that illustrated in Fig. 5b, Fig. 6b: the lines of constant poloidal field have straightened and become more z-independent, while the angular velocity is of large magnitude, and a large gradient is observed in $\psi r\sin\theta$ close to $r = 1$. At $B_p = 0.30 = B_p^{\min}$, both the evolution towards model-Z and Taylor states are of equal importance (Fig. 7b, Fig. 8b). This can be seen by examining the angular velocity. Neither a Taylor type flow (Fig. 3, which is predominantly geostrophic with a large positive region close to the rotation axis) nor a model-Z type flow (Fig. 6, which is again predominantly geostrophic, but flowing in the opposite direction) dominate. Instead, the net effect is that the geostrophic flows of Taylor and model-Z type cancel each other out and an underlying ageostrophic flow emerges, which is approximately 15 times weaker than either the Taylor ($B_p = 0.24$) or model-Z ($B_p = 0.60$) type flow.

Finally, for the other E illustrated in Fig. 4 and cases with $\omega_0 = 100$, 200, the same qualitative picture emerges; the evolution towards a Taylor state competes against model-Z, with Taylor-type features

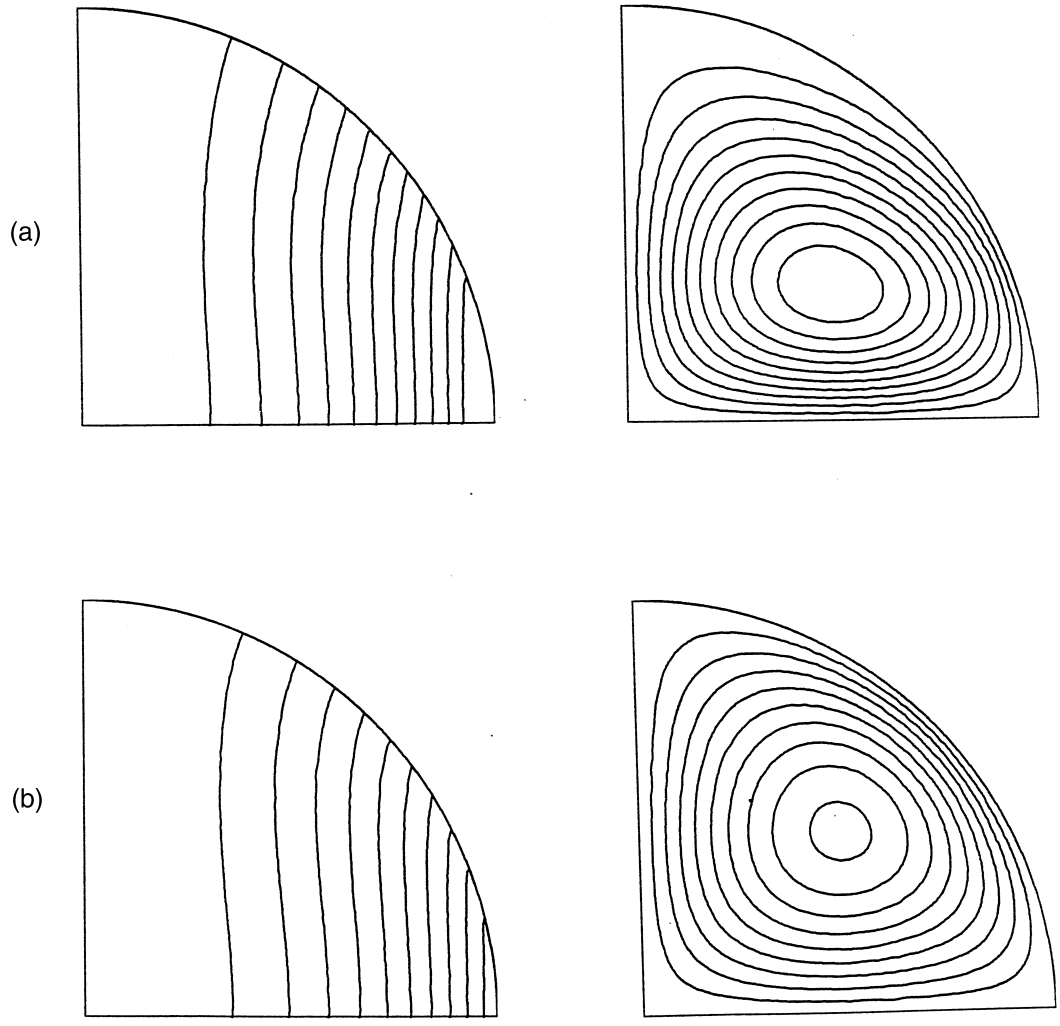

Fig. 7. Contour plots of the dimensionless equilibrated field with $\omega_0 = 400$, $C = 1/15$, $E = 10^{-8}$, ω given by Eq. (2.18a). Left-hand side illustrates $Ar\sin\theta$, right-hand side B. (a) $B_p = 0.24$, $(Ar\sin\theta)_{max} = 0.11$, $B_{max} = 0.935$; (b) $B_p = 0.30$ $(= B_p^{min})$, $(Ar\sin\theta)_{max} = 0.165$, $B_{max} = 1.65$.

preferred at small B_p and model-Z type features preferred at large B_p. (This is reminiscent, incidentally, of the result obtained by Roberts, 1989; Braginsky and Roberts, 1994 that their model also seemed to evolve from a Taylor state towards a model-Z state as their forcing was increased.) One final result is that for $\omega_0 \geq 200$, the position of B_p^{min} is independent of E but directly proportional to $\omega_0^{-1/2}$. This result can be understood by noting that for $\omega_0 \gg 1$, the magnetic wind (Eq. (2.9)) is dominated by the $M(B,B)$ term, since A scales as B_p whereas B scales as $\omega_0 B_p$. Thus, neglecting the $M(D^2A, A)$ term and following this scaling consistently throughout the steady-state equations, it turns out that ω_0 only enters through the combination $\omega_0 B_p^2$. Therefore, it is not unreasonable to expect some critical value of B_p to scale as $\omega_0^{-1/2}$.

3.3. The dependence on ω and C

We consider the dependence of the solution on the form of ω and A^*. With ω given by Eq. (2.18b), we repeat the computations described in Figs. 1 and 4. We find that exactly the same qualita-

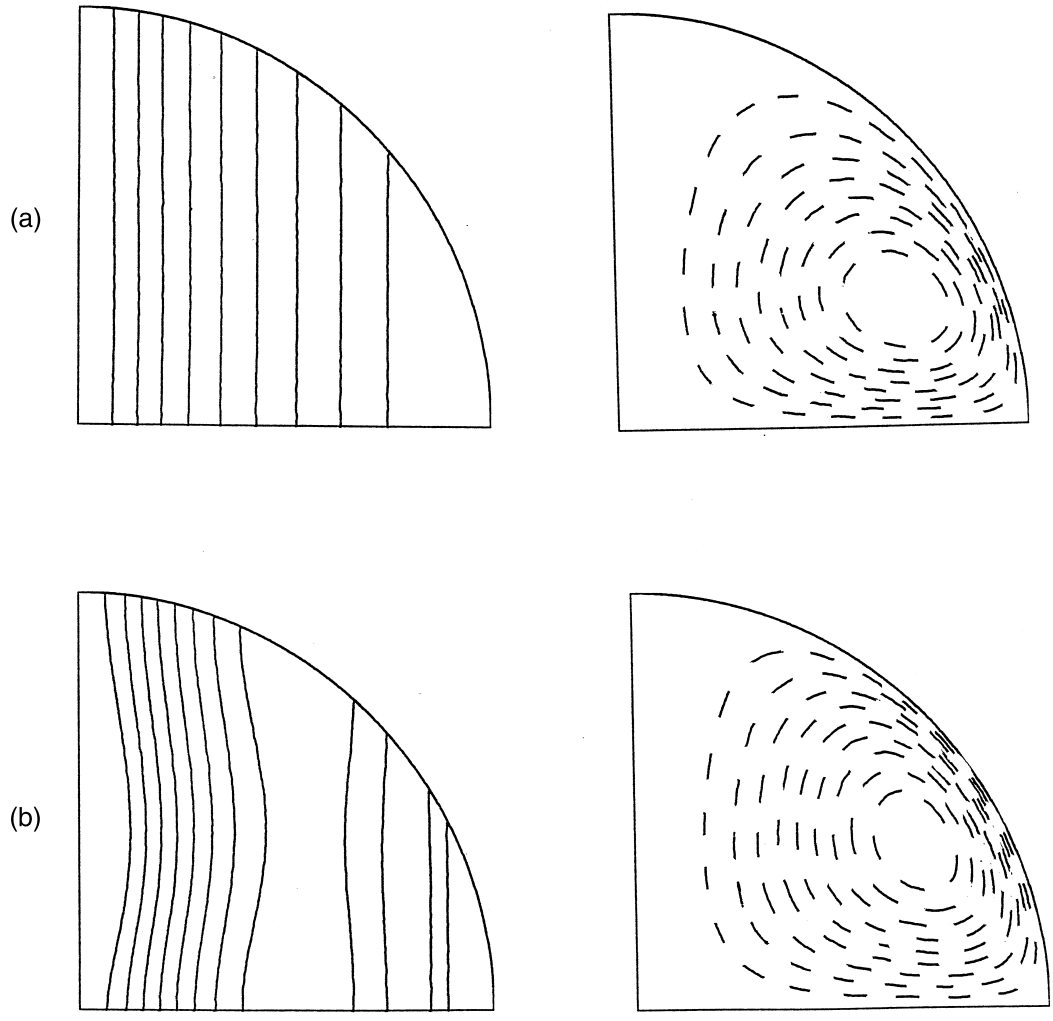

Fig. 8. The dimensionless flow corresponding to Fig. 7. Left-hand side illustrates $U/r\sin\theta$ ($U = U_m + U_g$), right-hand side $\psi r\sin\theta$. (a) $B_p = 0.24$, $(U/r\sin\theta)_{max} = 1500$, $(\psi r\sin\theta)_{min} = -0.12$; (b) $B_p = 0.30$ ($= B_p^{min}$), $(U/r\sin\theta)_{max} = 105$, $(\psi r\sin\theta)_{min} = -0.225$.

tive behaviour occurs in both cases: for $\omega_0 = 20$, the system tends towards a Taylor state as $B_p \to 1$ while for $\omega_0 = 400$, the approach towards a Taylor state competes with that of model-Z, with model-Z dominating at large B_p. Thus, we conclude that the functional form of ω is of secondary importance; the strength of ω, namely ω_0, is the key parameter which governs the evolution of the system.

Finally, once again, we repeat the simulations described in Figs. 1 and 4, but now return to the original choice of ω (Eq. (2.18a) and investigate the dependence of the solution on A^*. Here, we set $C = 2/15$, i.e., we double the amount of curvature in the imposed field. The picture that emerges is the same as that illustrated in Figs. 1 and 4. We conclude that the functional form of A^* is of secondary importance, it is the strength of A^*, namely B_p, which is the important parameter in determining the state of the final equilibrated solution.

4. Conclusion

In this work, we have pointed out that the adjustment to Taylor's constraint is considerably more

difficult in the presence of an ambient field, because once the ambient field is of strength greater than $E^{1/4}$, Ekman states are disallowed, and also because the field simply has less freedom to adjust. For weak thermal winds, we found that our particular model nevertheless manages to achieve a Taylor state. In contrast, for strong thermal winds, our model does not manage to achieve a Taylor state, but ultimately ends up in a model-Z state instead (although it has been suggested that for sufficiently small E, a model-Z state eventually becomes a Taylor state as well; Jault, 1995).

Returning to our original motivation—the magnetic fields of some of the Galilean moons of Jupiter—we can only broadly relate the numerical results described in this paper with the actual magnetic fields of the moons because (i) there is insufficient data to estimate accurately the dimensionless parameters appearing in the problem, e.g., the Ekman number E, or the strength of the thermal wind ω_0, and (ii) the model presented here is, obviously, an idealisation of the physical system. However, bearing this in mind, we speculate the following. Whether the Galilean moons are more likely to be in a model-Z or a Taylor state remains an open question, since the strength of the thermal wind is unknown. Also, even with the simplistic approach taken in this paper, we are still unable to reach the asymptotic limit relevant to the Galilean moons ($E \leq 10^{-13}$). Nevertheless, assuming we are in a strong thermal wind regime (which is probably the more likely scenario), and noting that B_p^{min} is proportional to $\omega_0^{-1/2}$ (B_p^{min} is the value of B_p at which model-Z begins to dominate, see Section 3), it would suggest that B_p^{min} occurs for a very weak imposed field. This in turn would suggest that model-Z may be preferred within the moons; however, we stress this point no further.

In conclusion, although this model is only applicable to the Jovian moons in a broad sense, even more caution should be taken here, than that already assumed for the Earth, in extrapolating from simulations at $E \geq O(10^{-4})$ to the systems of real interest.

Acknowledgements

One of us (M.R.W.) would like to thank Graeme Sarson and Richard Holme for useful comments. This work was supported by PPARC grant GR/K06495.

References

Barenghi, C.F., Jones, C.A., 1991. Nonlinear planetary dynamos in a rotating spherical shell: I. Numerical methods. Geophys. Astrophys. Fluid Dyn. 60, 211–243.

Braginsky, S.I., 1975. Nearly axially symmetric model of the hydrodynamic dynamo of the Earth I. Geomagn. Aeron. 15, 122–128.

Braginsky, S.I., 1994. The nonlinear dynamo and model-Z. In: Proctor, M.R.E., Gilbert, A.D. (Eds.), Stellar and Planetary Dynamos, CUP.

Braginsky, S.I., Roberts, P.H., 1994. From Taylor state to model-Z. Geophys. Astrophys. Fluid Dyn. 77, 3–13.

Cowling, T.G., 1934. The magnetic field of sunspots. Mon. Not. R. Astron. Soc. 94, 39–48.

Fearn, D.R., 1994. Nonlinear planetary dynamos. In: Proctor, M.R.E., Gilbert, A.D. (Eds.), Stellar and Planetary Dynamos, CUP.

Fearn, D.R., Proctor, M.R.E., 1992. Magnetostrophic balance in nonaxisymmetric, non-standard dynamo models. Geophys. Astrophys. Fluid Dyn. 67, 117–128.

Glatzmaier, G.A., Roberts, P.H., 1997. Simulating the geodynamo. Contemp. Phys. 38, 269–288.

Hollerbach, R., 1996. On the theory of the geodynamo. Phys. Earth Planet. Inter. 98, 163–185.

Hollerbach, R., 1997. The dynamical balance in semi-Taylor states. Geophys. Astrophys. Fluid Dyn. 84, 85–98.

Hollerbach, R., Ierley, G.R., 1991. A modal α^2 dynamo in the limit of asymptotically small viscosity. Geophys. Astrophys. Fluid Dyn. 56, 133–158.

Hollerbach, R., Jones, C.A., 1995. On the magnetically stabilizing role of the Earth's inner core. Phys. Earth Planet. Inter. 87, 171–181.

Hollerbach, R., Proctor, M.R.E., 1993. Non-axisymmetric shear layers in a rotating spherical shell. In: Proctor, M.R.E., Matthews, P.C., Rucklidge, A.M. (Eds.), Solar and Planetary Dynamos, CUP.

Hollerbach, R., Barenghi, C.F., Jones, C.A., 1992. Taylor's constraint in a spherical $\alpha\omega$-dynamo. Geophys. Astrophys. Fluid Dyn. 67, 3–25.

Jault, D., 1995. Model-Z by computation and Taylor's conditions. Geophys. Astrophys. Fluid Dyn. 79, 99–124.

Jones, C.A., Longbottom, A.W., Hollerbach, R., 1995. A self-consistent convection driven geodynamo model, using a mean field approximation. Phys. Earth Planet. Inter. 92, 119–141.

Khurana, K.K., Kivelson, M.G., Russell, C.T., Walker, R.J., Southwood, D.J., 1997. Absence of an internal magnetic field at Callisto. Nature 387, 262–264.

Khurana, K.K., Kivelson, M.G., Stevenson, D.J., Schubert, G., Russell, C.T., Walker, R.J., Polanskey, C., 1998. Induced magnetic fields as evidence for subsurface oceans in Europa and Callisto. Nature 395, 777–780.

Kivelson, M.G., Khurana, K.K., Walker, R.J., Russell, C.T., Linker, J.A., Southwood, D.J., Polanskey, C., 1996a. A magnetic signature at Io: initial report from the Galileo magnetometer. Science 273, 337–340.

Kivelson, M.G., Khurana, K.K., Russell, C.T., Walker, R.J., Warnecke, J., Coroniti, F.V., Polanskey, C., Southwood, D.J., Schubert, G., 1996b. Discovery of Ganymede's magnetic field by the Galileo spacecraft. Nature 384, 537–541.

Kuang, W., Bloxham, J., 1997. An Earth-like numerical dynamo model. Nature 377, 203–209.

Roberts, P.H., 1972. Kinematic dynamo models. Philos. Trans. R. Soc. A 272, 663–698.

Roberts, P.H., 1989. From Taylor state to model-Z?. Geophys. Astrophys. Fluid Dyn. 49, 143–160.

Russell, C.T., 1993. Magnetic fields of the terrestrial planets. J. Geophys. Res. E 98, 18681–18695.

Sarson, G.R., Jones, C.A., Zhang, K., Schubert, G., 1997. Magnetoconvection dynamos and the magnetic fields of Io and Ganymede. Science 276, 1106–1108.

Sarson, G.R., Jones, C.A., Zhang, K., 1999. Dynamo action in a uniform ambient field. Phys. Earth Planet. Inter. 111, 47–68.

Taylor, J.B., 1963. The magnetohydrodynamics of a rotating fluid and the Earth's dynamo problem. Proc. R. Soc. London A 274, 274–283.

Walker, M.R., Barenghi, C.F., 1998. Accurate numerical computations of Taylor integrals. Geophys. Astrophys. Fluid Dyn. 87, 173–191.

Walker, M.R., Barenghi, C.F., Jones, C.A., 1998. A note on dynamo action at asymptotically small Ekman number. Geophys. Astrophys. Fluid Dyn. 88, 261–275.

Zhang, K., Jones, C.A., 1997. The effect of hyperviscosity on geodynamo models. Geophys. Res. Lett. 24, 2869–2872.